



SCUOLA INTERNAZIONALE SUPERIORE DI STUDI AVANZATI

SISSA Digital Library

Shedding Plasma Membrane Vesicles Induced by Graphene Oxide Nanoflakes in Brain Cultured Astrocytes

*Original*

Shedding Plasma Membrane Vesicles Induced by Graphene Oxide Nanoflakes in Brain Cultured Astrocytes / Musto, Mattia; Parisse, Pietro; Pachetti, Maria; Memo, Christian; Di Mauro, Giuseppe; Ballesteros, Belen; Lozano, Neus; Kostarelos, Kostas; Casalis, Loredana; Ballerini, Laura. - In: CARBON. - ISSN 0008-6223. - 176:(2021), pp. 458-469. [10.1016/j.carbon.2021.01.142]

*Availability:*

This version is available at: 20.500.11767/118246 since: 2021-02-09T10:13:15Z

*Publisher:*

*Published*

DOI:10.1016/j.carbon.2021.01.142

*Terms of use:*

Testo definito dall'ateneo relativo alle clausole di concessione d'uso

*Publisher copyright*  
Elsevier

This version is available for education and non-commercial purposes.

note finali coverpage

(Article begins on next page)

# Journal Pre-proof

Shedding Plasma Membrane Vesicles Induced by Graphene Oxide Nanoflakes in Brain Cultured Astrocytes

Mattia Musto, Pietro Parisse, Maria Pachetti, Christian Memo, Giuseppe Di Mauro, Belen Ballesteros, Neus Lozano, Kostas Kostarelos, Loredana Casalis, Laura Ballerini

PII: S0008-6223(21)00162-7

DOI: <https://doi.org/10.1016/j.carbon.2021.01.142>

Reference: CARBON 16070

To appear in: *Carbon*

Received Date: 4 December 2020

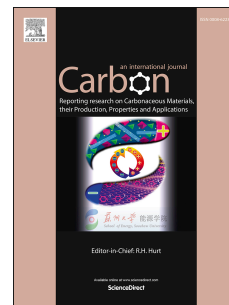
Revised Date: 25 January 2021

Accepted Date: 27 January 2021

Please cite this article as: M. Musto, P. Parisse, M. Pachetti, C. Memo, G. Di Mauro, B. Ballesteros, N. Lozano, K. Kostarelos, L. Casalis, L. Ballerini, Shedding Plasma Membrane Vesicles Induced by Graphene Oxide Nanoflakes in Brain Cultured Astrocytes, *Carbon*, <https://doi.org/10.1016/j.carbon.2021.01.142>.

This is a PDF file of an article that has undergone enhancements after acceptance, such as the addition of a cover page and metadata, and formatting for readability, but it is not yet the definitive version of record. This version will undergo additional copyediting, typesetting and review before it is published in its final form, but we are providing this version to give early visibility of the article. Please note that, during the production process, errors may be discovered which could affect the content, and all legal disclaimers that apply to the journal pertain.

© 2021 The Author(s). Published by Elsevier Ltd.



# Shedding Plasma Membrane Vesicles Induced by Graphene Oxide Nanoflakes in Brain Cultured Astrocytes

*Mattia Musto<sup>1†</sup>, Pietro Parisse<sup>2</sup>, Maria Pachetti<sup>2</sup>, Christian Memo<sup>1</sup>, Giuseppe Di Mauro<sup>1</sup>,  
Belen Ballesteros<sup>3</sup>, Neus Lozano<sup>3</sup>, Kostas Kostarelos<sup>3,4</sup>, Loredana Casalis<sup>2\*</sup> and Laura  
Ballerini<sup>1\*</sup>*

<sup>1</sup>International School for Advanced Studies (SISSA), 34136 Trieste, Italy

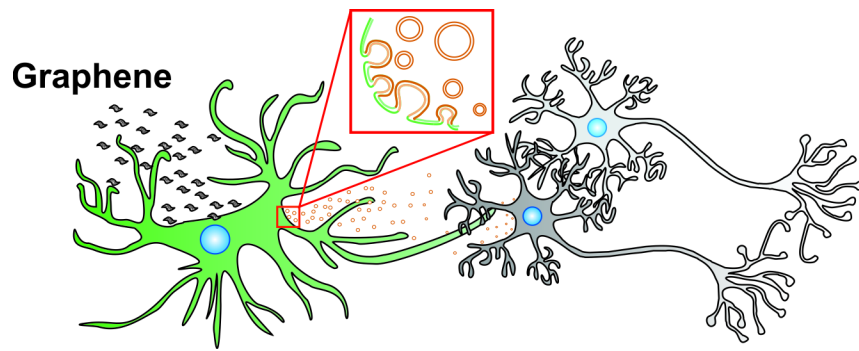
<sup>2</sup>ELETTRA Synchrotron Light Source, 34149 Basovizza, Italy

<sup>3</sup>Catalan Institute of Nanoscience and Nanotechnology (ICN2), Campus UAB, Bellaterra,  
08193 Barcelona, Spain

<sup>4</sup>Nanomedicine Lab, National Graphene Institute and Faculty of Biology, Medicine & Health  
The University of Manchester, Manchester M13 9PT, United Kingdom

## **Credit Author Statements**

M.M. performed cell biology, electrophysiology, and immunofluorescence experiments and analysis; M.M. and P.P. designed and performed AFM experiments; M.P. performed IR and UVRR experiments and analysis. CM and GDM performed biology and WB experiments; N.L. and K.K. contributed to the synthesis and characterization of thin graphene oxide of biological grade. BB performed SEM micrographs of GO. L.B. and L.C. conceived the study; L.B. conceived the experimental design and contributed to the analysis of data; L.B. wrote the manuscript.



Journal Pre-proof

# Shedding Plasma Membrane Vesicles Induced by Graphene Oxide Nanoflakes in Brain Cultured Astrocytes

*Mattia Musto<sup>1†</sup>, Pietro Parisse<sup>2</sup>, Maria Pachetti<sup>2</sup>, Christian Memo<sup>1</sup>, Giuseppe Di Mauro<sup>1</sup>, Belen Ballesteros<sup>3</sup>, Neus Lozano<sup>3</sup>, Kostas Kostarelos<sup>3,4</sup>, Loredana Casalis<sup>2\*</sup> and Laura Ballerini<sup>1\*</sup>*

<sup>1</sup>International School for Advanced Studies (SISSA), 34136 Trieste, Italy

<sup>2</sup>ELETTRA Synchrotron Light Source, 34149 Basovizza, Italy

<sup>3</sup>Catalan Institute of Nanoscience and Nanotechnology (ICN2), Campus UAB, Bellaterra, 08193 Barcelona, Spain

<sup>4</sup>Nanomedicine Lab, National Graphene Institute and Faculty of Biology, Medicine & Health The University of Manchester, Manchester M13 9PT, United Kingdom

## Abstract

Microvesicles (MVs) generated and released by astrocytes, the brain prevalent cells, crucially contribute to intercellular communication, representing key vectorized systems able to spread and actively transfer signaling molecules from astrocytes to neurons, ultimately modulating target cell functions. The increasing clinical relevance of these signaling systems requires a deeper understanding of MV features, currently limited by both their nanoscale dimensions and the low rate of their constituent release. Hence, to investigate the features of such glial signals, nanotechnology-based approaches and the applications of unconventional, cost-effective tools in generating MVs are needed. Here, small graphene oxide (s-GO) nanoflakes are used to boost

22 MVs shedding from astrocytes in cultures and s-GO generated MVs are compared with those  
23 generated by a natural stimulant, namely ATP, by atomic force microscopy, light scattering,  
24 attenuated total reflection–fourier transform infra-red and ultraviolet resonance Raman  
25 spectroscopy. We also report the ability of both types of MVs, upon acute and transient exposure  
26 of patch clamped cultured neurons, to modulate basal synaptic transmission, inducing a stable  
27 increase in synaptic activity accompanied by changes in neuronal plasma membrane elastic  
28 features.

29  
30 **Keywords:** graphene oxide, extracellular vesicles, atomic force microscopy and spectroscopy,  
31 FTIR-ATR and UVRR spectroscopy, synaptic activity, cortical neuronal cultures

32

### 33 **1. Introduction**

34 In biology, newly described forms of intercellular communication comprise the release of  
35 vesicles, named extracellular vesicles, from virtually all cell types, including resident glial cells  
36 of the central nervous system (CNS), such as astrocytes and microglia.[1,2] In particular, the  
37 shedding of membrane vesicles is a recognized form of cross talk in the multidimensional  
38 signaling between astrocytes, (i.e. the majority of cells in the mammalian CNS), and neurons in  
39 physiology, but also in neurodegenerative and neuroinflammatory diseases as well as in brain  
40 tumors. Extracellular vesicle signaling molecules, either stored within their cargo or embedded in  
41 their plasma membrane, modulate relevant processes in the development, physiology and  
42 pathology of CNS target cells.[3–6] The signaling system based on release of extracellular  
43 vesicles comprises shedding microvesicles (MV) and exosomes, characterized by different size,  
44 membrane composition, cargo and origin.[7,8]

45 MVs are nanovesicles able to interact specifically with cells at local or distant sites.[9] In  
46 maintaining CNS functions, glial cells intensely communicate with neurons, also *via* the release  
47 of MVs, which represents a highly versatile tool to functionally impact the CNS.[10–12] MVs  
48 are considered a “vectorized” signaling system able to bind their target cells to transmit specific  
49 information. The reported spreading ability of MVs has suggested their potential exploitation as  
50 biomarkers or as engineered therapeutic carriers.[13] A comprehensive correlation between  
51 conditions used to release and harvest MVs from the same cell type, i.e. astrocytes, and their  
52 signaling ability, will impact our understanding of MVs physiology and the design of MV-based  
53 biomedical applications in the CNS.[14,15] Particular attention has to be conveyed to devise  
54 novel, cost-effective ways in generating MVs, in particular enhancing constitutive release.

55 Here, we concentrate on graphene oxide (GO), the most common derivative of graphene,  
56 whose properties can be tailored to adapt to new physical and biological applications.[16,17] GO  
57 flakes have been successfully designed for drug delivery applications in biomedicine.[18] In the  
58 CNS, small GO nano-flakes (s-GO) were shown to induce constitutive MV release from cultured  
59 astrocytes and to potentiate evoked MV release induced upon exposure to bzATP.[19] s-GO  
60 flakes, due to their physical features at the nanoscale, were reported to interfere with cellular  
61 membrane dynamics.[19,20] In addition, *via* adhesion to the plasma membrane, s-GO may alter  
62 the mechanical features of the lipid bilayer[21] triggering genuine biological responses, such as  
63 MVs signaling. Thus s-GOs may represent a tool to exploit mechanical signaling at the  
64 nanoscale to activate membrane release of MVs. Drug delivery applications where vesicle  
65 release from genetically engineered cells is required, may take advantage of the mechanical  
66 modulation of vesicle release brought about by graphene-based nanomaterials, representing a  
67 safer and cheaper alternative to pharmacological tools. Prolonged exposure to biomolecules able

68 to induce MVs release, such as ATP, could in fact negatively affect cell physiology by  
69 promoting astrogliosis and inducing microglia-mediated neuroinflammatory responses.[22]

70 We use the ability of s-GO to substantially increase the production of MVs from astrocytes to  
71 provide, for the first time, a robust and comparative vesicle characterization by means of ultra-  
72 microscopy, attenuated total reflection–fourier transform infra-red (FTIR-ATR) and UV  
73 Resonant Raman (UVRR) spectroscopy. We additionally explore by single cell patch-clamp  
74 recordings the impact of acute, local and transient delivery of MVs on neuronal basal synaptic  
75 activity and by atomic force microscopy (AFM) the accompanying changes in neuronal plasma  
76 membrane elastic features.

## 77 **2. Material and Methods**

### 78 *2.1 Graphene oxide nanosheets synthesis*

79 GO was manufactured under endotoxin-free conditions through our modified Hummers' method  
80 as previously described.[19] The complete characterization of the material used is shown and  
81 summarised in the Supplementary experimental section and Supplementary Figure S1 and Table  
82 S1.

### 83 *2.2 Cell Cultures*

84 All experiments were performed in accordance with the EU guidelines (Directive 2010/63/EU)  
85 and Italian law (decree 26/14) and were approved by the local authority veterinary service and by  
86 our institution (SISSA-ISAS) ethical committee. All efforts were made to minimize animal  
87 suffering and to reduce the number of animals used. Animal use was approved by the Italian  
88 Ministry of Health, in agreement with the EU Recommendation 2007/526/EC.

89 Primary glial cultures were obtained from cortices isolated from neonatal rats (Wistar) at  
90 postnatal day 2-3 (P2–P3), as previously described [19,23]. Dissociated cells were plated into

91 plastic 150 cm<sup>2</sup> flasks and incubated at 37 °C; 5 % CO<sub>2</sub> in culture medium composed of DMEM  
92 (Invitrogen), supplemented with 10 % fetal bovine serum (FBS; Thermo Fisher), 100 IU/ mL  
93 penicillin, and 10 mg/mL streptomycin.

94 Cortical neurons were isolated from neonatal rat cortices (Wistar) at postnatal day 0-1  
95 (P0–P1). Dissociated cells were then plated on poly-L-ornithine (Sigma) coated coverslips  
96 (Kindler, EU) at a concentration of 150000 cells in a volume of 200 µL and incubated at 37 °C; 5  
97 % CO<sub>2</sub> in a culture medium composed of Neurobasal-A (Thermo Fischer) containing 2% B27  
98 (Gibco), 10 mM Glutamax and 0.5 µM Gentamycin (Gibco) for 8-10 *days in vitro* (DIV) before  
99 performing electrophysiological experiments.

### 100 2.3 MV Isolation

101 MV shedding and isolation was performed as previously described.[19] One pool of MVs  
102 were collected from 21-24 DIV glial cultures previously treated with graphene oxide nanoflakes  
103 (s-GO) (10 µg/mL[19]), added to culture medium once and left for 6 days. At the end of 6-days  
104 exposure, the medium was removed and substituted with physiological saline solution, with the  
105 following composition: 152 mM NaCl, 4 mM KCl, 1 mM MgCl<sub>2</sub>, 2 mM CaCl<sub>2</sub>, 10 mM HEPES  
106 and 10 mM Glucose (pH adjusted to 7.4), at 37 °C and 5 % CO<sub>2</sub> for 60 min prior to MVs  
107 collection and purification. The MVs pool was isolated from cultures treated (30 min) with  
108 benzoyl-ATP (bzATP; 100 µM) diluted in physiological saline solution. The 6-days exposure  
109 timepoint was chosen on the basis of previous western blot experiments, and confirmed by our  
110 current experiments testing MVs release after 3 days of s-GO exposure (supplementary Figure  
111 S2).[19] Negative controls were incubated with physiological solution without the presence of  
112 bzATP or s-GO. After the incubation period, cell medium was collected and centrifuged for 15  
113 min at a speed of 300 × g in order to remove cell debris. Supernatant was then collected and

114 MVs were pelleted by centrifugation at  $20000 \times g$  for 2 hours. For  $Ca^{2+}$  deprivation experiments,  
115 prior to supernatant collection and MVs pellet centrifugation, cultures were pre-incubated for 45  
116 min in a saline solution identical to the physiological saline solution except for 0 mM  $CaCl_2$ , 3  
117 mM  $MgCl_2$  and 1mM EGTA to allow the depletion of intracellular calcium storage. Upon this  
118 pre-treatment, we harvest the MVs from controls, s-GO treated and bzATP (30 min in  $Ca^{2+}$   
119 deprived solution; supplementary Figure S3).

#### 120 *2.4 Western blot analysis*

121 MVs were prepared as previously reported, briefly they were re-suspended in lysis buffer (50  
122 mM Tris-HCl, pH 8.0, 150 mM NaCl, 1 % NP40, 0.1 % SDS), sonicated for 30 s, and then  
123 boiled at 95 °C for 5 min.[19] Samples were run on a 10 % polyacrylamide gel and blotted onto  
124 nitrocellulose membranes (Millipore, Italy). Membranes were then blocked in PBS-Tween-20  
125 (0.1 %) plus 5 % nonfat dry milk and incubated with the primary antibody antitubulin-1 (dilution  
126 1:1000) for 16 h at 4 °C. Membranes were then washed with PBS-Tween and incubated with  
127 peroxidase-conjugated anti-mouse secondary antibody (dilution 1:1000). Detection of  
128 immunolabeled ECL-exposed protein bands was measured with UVI-1D software over three  
129 independent experiments.

#### 130 *2.5 Immunofluorescence and confocal microscopy*

131 Primary glial and cortical neurons cultures were fixed in 4 % formaldehyde (PFA, prepared  
132 from fresh paraformaldehyde) in PBS for 20 min at room temperature (RT) and then washed in  
133 PBS. Free aldehyde groups were quenched in 0.1 M glycine solution for 5 min. The samples  
134 were permeabilized in 5 % fetal bovine serum (FBS), 0.3 % Triton-X 100 in phosphate buffer  
135 solution (PBS) for 30 min at RT. Samples were then incubated with primary antibodies (mouse  
136 monoclonal anti-GFAP, Invitrogen, 1:500 dilution; rabbit polyclonal anti- $\beta$ -tubulin III, Sigma-

137 Aldrich, 1:500 dilution) diluted in PBS with 5 % FBS at 4 °C for 1 hours. Samples were then  
138 incubated with secondary antibodies (Alexa 488 goat anti-mouse, Invitrogen, 1:500 dilution;  
139 Alexa 594 goat anti-rabbit, Invitrogen, 1:500 dilution), and DAPI (Invitrogen, dilution 1:200) to  
140 stain the nuclei, for 45 min at RT and finally mounted on 1 mm thick glass coverslips using  
141 Fluoromount mounting medium (Sigma-Andrich). Images were acquired using a Nikon C2  
142 Confocal, equipped with Ar/Kr, He/Ne and UV lasers with a 40 × or 60 × (1.4 NA) oil-objective  
143 (using oil mounting medium, 1.515 refractive index) to acquire glial cultures images and cortical  
144 neurons images respectively. 200 × 200 μm fields were acquired for cortical neurons images and  
145 300 × 300 μm fields were acquired for glial cells images. Confocal sections were acquired every  
146 0.25 μm for both the cultures.

#### 147 *2.6 Glial cell viability assay*

148 Primary rat astrocytes (21-24 DIV) were exposed to s-GO 10 μg/mL or to equivalent volumes  
149 of the vehicle for 6 days. Cells were stained with propidium iodide (PI, 1 μg/ml; 15 min) for cell  
150 death quantification and subsequently fixed in PFA and labelled for DAPI for nuclei  
151 visualization and GFAP for visualizing astrocytes. The red (PI positive) fluorescent nuclei  
152 indicating dead cells were quantified at 40 × (1.4 NA) magnification using a Nikon C2 Confocal  
153 microscope, equipped with Ar/Kr, He/Ne and UV lasers, with random sampling of 10 fields per  
154 sample (n = 3 coverslips/sample, from 3 independent culture preparations). The average  
155 percentage of dead cells was calculated counting visual fields selected.

#### 156 *2.7 FM1-43 staining*

157 Glial cells were incubated with the fluorescent styryl dye FM1-43 (2 μM) for 2 min in order to  
158 completely stain plasma membrane, then extensively washed with PBS and exposed for 30 min  
159 to bzATP (100 μM) or to standard saline solution.[19] Samples were placed in a recording

160 chamber mounted on an inverted microscope (Nikon Eclipse Ti-U) and observed with a  $40 \times$   
161 objective (0.6 NA, PlanFluor, Nikon). Images ( $512 \times 512$  px) were acquired for 10 min with an  
162 exposure time of 150 ms (6.6 Hz) by a Hamamatsu Orca-Flash 4.0 digital camera controlled by  
163 an integrating imaging software package (HCImage, Hamamatsu). Recorded images were  
164 analyzed offline with the Clampfit software (pClamp suite, 10.2 version; Axon Instruments).  
165 Image time stacks were analyzed in selected regions of interest (ROI) to measure the  
166 variations in FM1-43 fluorescence intensity over time. Natural sample bleaching over time,  
167 due to prolonged light exposure, has the same time-course and intensity in all the three  
168 groups, as previously described[19].

#### 169 *2.8 Atomic Force Microscopy Analysis*

170 AFM characterization was performed as previously described.[19] Briefly, the pellet of MVs  
171 was re-suspended in PBS solution after isolation from cell cultures and a  $15 \mu\text{L}$  drop of sample  
172 solution was placed and left to adsorb (30 min) onto a freshly peeled mica substrate. Vesicles  
173 were then fixed with 1% formaldehyde for 1 h (RT) in order to prevent their collapse during  
174 AFM acquisition. MVs were then washed with PBS and dried under a gentle stream of nitrogen.  
175 AFM analysis was performed in air at RT, using the semicontact mode of a commercial  
176 instrument (Solver Pro, NT-MDT, RU). Silicon tips (NSC36/CR-AU, MikroMash, USA) with a  
177 typical force constant of  $0.6 \text{ nN/nm}$  and a resonance frequency of about 65 kHz were employed.  
178 Topographic height and phase images were recorded at  $512 \times 512$  pixels at a scan rate of 0.5 Hz.  
179 Image processing was performed using Gwyddion freeware AFM analysis software, version  
180 2.40. Diameter and height of each vesicle were evaluated from cross-line profiles, and results  
181 were statistically analyzed using Prism (Graphpad software).

#### 182 *2.9 Neuronal Stiffness*

183 9-10 DIV cortical neurons were exposed to MVs obtained by glial cultures treated with bzATP  
184 or s-GO and neuronal rigidity was assessed with AFM, 24 hours after MVs exposure. Force  
185 spectroscopy measurements were performed with a commercial Smena AFM (NT-MDT, RU)  
186 mounted on an inverted microscope (Nikon Eclipse Ti-U). AFM cantilever deflection was  
187 measured when pushed against cortical neurons plated on a glass coverslip. Deflection values  
188 were subsequently converted into a force versus indentation curve based on cantilever spring  
189 constant and its displacement. Neuronal rigidity was evaluated in 50 randomly chosen neurons  
190 for each condition (from 3 independent experiments), acquiring three force spectroscopy curves  
191 in the center of each cell soma. The AFM tip was positioned by using an inverted microscope in  
192 bright field mode.

193 AFM micro-cantilevers with an elastic constant of about 0.03 nN/nm and a resonance  
194 frequency of about 10 kHz (CSG01 tipless cantilevers from NT-MDT, RU) were used. A  
195 borosilicate glass microsphere of about 18  $\mu\text{m}$  in diameter ( $18.2 \pm 1.0 \mu\text{m}$  from Duke Standards,  
196 CA, USA) was manually glued at the end of each cantilevers using a UV curable glue (Norland  
197 Optical Adhesive 61 from Norland Products Inc., NJ, USA). Force spectroscopy measurements  
198 were performed at a constant indentation speed of 1 mm/s with a maximum value of indentation  
199 deepness set at 500 nm. Elastic modulus values (E), expressed in kPa, were determined by fitting  
200 obtained force-indentation curves with a Hertzian model for the tip, using AtomicJ (v. 1.7.3)  
201 analysis software.[24]

#### 202 *2.10 Nanoparticle Tracking analysis (NTA)*

203 Measurement and analysis of MVs size distribution by NTA was performed on a NanoSight  
204 LM10 system (Malvern) using approximately 500  $\mu\text{L}$  of MVs of both conditions (bzATP-  
205 derived and s-GO-derived) diluted 1:20 in MilliQ  $\text{H}_2\text{O}$ . Individual videos of 60 seconds

206 (recorded at 25 FPS; 3 videos per group) for each sample were acquired at RT using the  
207 maximum camera gain, a detector threshold equal to 8 and analyzed by the NanoSight particle  
208 tracking software to calculate size and vesicle concentration.

### 209 *2.11 FTIR-ATR Spectroscopy and UV Resonant Raman (UVR) Measurements*

210 MVs were isolated from 21-24 DIV glial cultures by centrifugation as described above. MVs  
211 pellet was successively washed with NaCl solution (150 mM) and finally re-suspended in 50  $\mu\text{L}$   
212 of the same solution in order to avoid contribution of phosphate and sugar groups to the IR  
213 absorbance spectra. The IR measurements were carried out at the BL10.2-IUVS beamline at  
214 Elettra synchrotron Trieste. The spectra were collected in ATR mode using a MIR DLaTGS  
215 detector and a KBr-broadband beam-splitter. For each IR measurement, 2  $\mu\text{L}$  of sample solution  
216 were spread over the whole area of a monolithic diamond ATR plate and left to dry forming a  
217 thin film. For each sample, 20 spectra were collected in the range  $4000\text{-}800\text{ cm}^{-1}$ , accumulating  
218 256 scans for each spectrum reaching a resolution of  $4\text{ cm}^{-1}$ . Each spectrum was corrected for the  
219 background, aqueous vapor,  $\text{CO}_2$  and not normalized to any absorbance band.

220 UVR measurements were performed at the BL10.2-IUVS beamline at Elettra synchrotron  
221 Trieste using the experimental set-up reported.[25] 5  $\mu\text{L}$  of vesicles solution were drop-casted  
222 onto an aluminum foil, allowed to dry and kept under nitrogen purging. All the measurements  
223 were performed at RT, using an excitation wavelength of 244 nm and tuning the power of the  
224 incoming radiation to 50  $\mu\text{W}$ . The outgoing radiation was collected in backscattering geometry  
225 by using a triple stage spectrometer (Trivista, Princeton Instrument) with a spectral resolution of  
226  $8\text{ cm}^{-1}$ . Samples were continuously oscillated horizontally in order to avoid photodamaging.

### 227 *2.12 Electrophysiological Recordings*

228 Patch-clamp recordings (whole-cell, voltage clamp mode) were performed from visually  
229 identified (under differential interference contrast - DIC - microscopy) cortical neurons (DIV 8-  
230 10) placed in a recording chamber, mounted on an inverted microscope (Eclipse Ti-U, Nikon,  
231 Japan) and superfused with control physiological saline solution of the following composition (in  
232 mM): 152 NaCl, 4 KCl, 1 MgCl<sub>2</sub>, 2 CaCl<sub>2</sub>, 10 HEPES and 10 Glucose (pH adjusted to 7.4 by  
233 NaOH 1M; osmolarity 300 mOsm). Cells were patched with glass pipettes (4-7 MΩ) containing  
234 (in mM): 120 K gluconate, 20 KCl, 10 HEPES, 10 EGTA, 2 MgCl<sub>2</sub> and 2 Na<sub>2</sub>ATP (pH adjusted  
235 to 7.35 by KOH; osmolarity 298 mOsm). All electrophysiological recordings were performed at  
236 RT and the spontaneous, basal synaptic activity was recorded by clamping the membrane voltage  
237 at -70 mV (corrected for liquid junction potential, which was -14 mV). To investigate the acute  
238 effect on synaptic activity of glia-derived MVs, an injection pipette (patch pipette with resistance  
239 of 1-4 MΩ) filled with MVs previously isolated glial cultures as described above and re-  
240 suspended in 100 μL of extracellular saline solution was positioned at 200 μm from the cell soma  
241 and connected to a pico-spritzer (PDES-02DX, npi Electronics) with 0.3 psi in-line pressure.[19]  
242 On the basis of MVs quantification obtained by NTA measurements, and considering that MVs  
243 isolation was performed using the same protocol in all the experiments described, we calculated  
244 that the concentration of MVs used for these tests was approximately of  $6.64 \times 10^9$  for MVs  
245 obtained by bzATP stimulation and  $1.64 \times 10^{10}$  for MVs isolated from s-GO treated cultures.  
246 Baseline spontaneous synaptic activity was recorded for the 10 min prior delivering the puff  
247 (500 ms duration) of MVs and followed up for 20 min to verify changes in post synaptic current  
248 (PSC) frequency and amplitude induced by the fusion of MVs with neuronal membranes.

249 Data were collected by Multiclamp 700B patch amplifier (Axon CNS, Molecular Devices) and  
250 digitized at 10 kHz with the pClamp 10.2 software (Molecular Devices LLC, USA). All

251 recorded events were analyzed offline with the AxoGraph 1.4.4 (Axon Instrument) event  
252 detection software (Axon CNS, Molecular Devices).

### 253 *2.13 Statistical Analysis*

254 Data sets found to follow a non-normal distribution, were represented as box plot. The central  
255 thick horizontal bar in the box plots indicates the median value, while the boxed area extends  
256 from the 25<sup>th</sup> to 75<sup>th</sup> percentiles with the whiskers ranging from the 2.5<sup>th</sup> to the 97.5<sup>th</sup> percentiles.  
257 Statistically significant differences between two non-parametric data sets were assessed by  
258 Mann-Whitney's test, while to assess statistically significant differences among three data-set we  
259 used the Kruskal-Wallis test and Dunn's post hoc test.  $P < 0.05$  was considered at a statistically  
260 significant.

261

## 262 **3. Results and discussion**

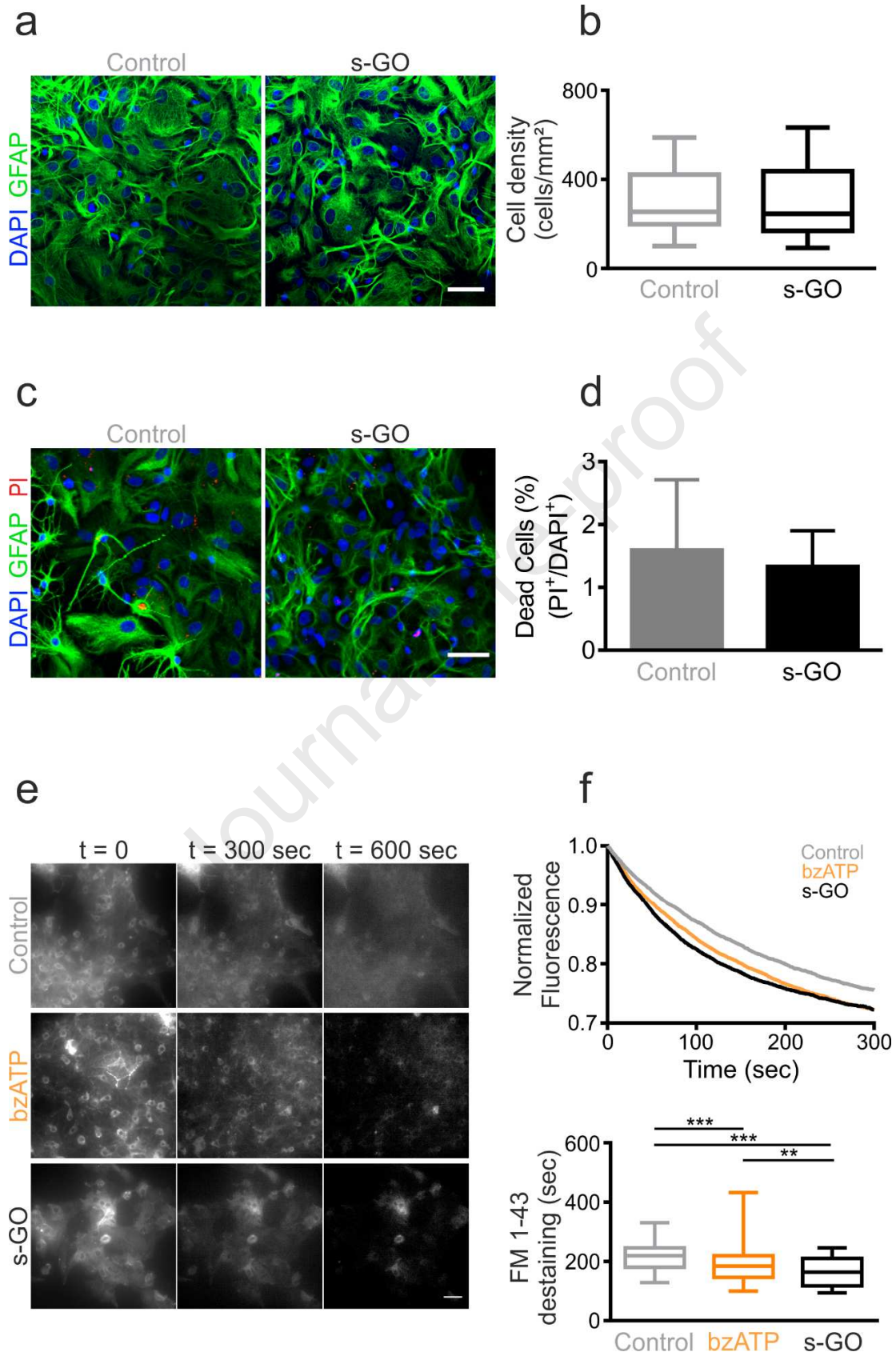
263 Astrocytes were isolated from postnatal (2-3 days) rat (Wistar) cortices, as previously  
264 described.[19,20,23] We used visually homogenous s-GO dispersions containing s-GO  
265 nanosheets with lateral dimensions predominantly between 50 – 500 nm.[19,20] We treated pure  
266 glial cell cultures with s-GO (10  $\mu\text{g}/\text{mL}$ ) for 6 days.[19] Immunofluorescence labeling by antigen  
267 against glial-fibrillary acidic protein (GFAP), an intermediate filament protein that is highly  
268 specific for cells of the astroglial lineage, was used to visualize control and s-GO-treated  
269 neuroglial cultures (GFAP, in green; Fig. 1a).[26] At the low concentrations used, s-GO  
270 treatment did not impair astrocyte morphology and cell density when compared with matched  
271 control cultures (box-plot in Fig. 1b).[19,27] Viability of glial cells was confirmed by propidium  
272 iodide (PI) cell death assay. Control and s-GO treated cultures were incubated with PI, which  
273 stain dead cells nuclei (Figure 1c, in red) and the percentage of PI-positive nuclei was calculated

274 (bar plot in Fig. 1d). Graphene nanosheets cytotoxicity is a largely debated issue, due to the  
275 variable impact on cell toxicity of several material's features, related either on the GO physical-  
276 chemical properties (thickness, size, surface functionalization, aggregation state and  
277 concentration) or on the synthesis method[28,29], the experimental conditions adopted here and  
278 in our previous works[19,20] exclude any cytotoxic effect on glial cells or neurons, both *in vitro*  
279 and *in vivo*.

280 MVs are released into the extracellular space by direct budding from the plasma membrane of  
281 astrocytes.[30] To explore the dynamics of MVs release in control, in s-GO treated and in ATP  
282 treated (see below) astrocytes, we measured the presence of changes in membrane trafficking by  
283 briefly incubating cultures with the fluorescent styryl dye FM1-43 and then quantifying the  
284 astrocyte-membrane fluorescence decay to provide a cumulative measure of exocytosis in the  
285 different growth conditions.[19,30]

286 FM dyes are fluorescent probes that reversibly stain membranes, and are largely used for  
287 optical real-time measurements of membrane dynamics and secretory processes.[31–33]  
288 Incubation with the FM dye (2  $\mu$ M, 2 min) resulted in clear surface membrane staining of  
289 control, bzATP, an agent known to evoke massive MVs release (100  $\mu$ M, 30 min) and s-GO  
290 treated cultures (10  $\mu$ g/mL, 6 days), highlighted in Figure 1e (left panels).[30] Brighter spots  
291 were considered as adherent debris and were excluded from the analysis. Besides these, both  
292 bright and weak FM-stained plasma membrane domains were present along the whole  
293 cytoplasmic surface and became visible within 2 min incubation (Fig. 1e). Due to this initial  
294 variability in the intensity of the membrane staining, all FM de-staining measures were  
295 normalized to the relative time 0. Once astrocyte membranes were labeled by the fluorescent dye  
296 FM1-43 we measured the plasma membrane de-staining over a fixed time (10 min) in control, in

297 s-GO treated cultures, or during acute exposure to bzATP, under the same culturing  
298 conditions.[19] Representative fluorescence intensity traces are shown in Figure 1f (top plot); the  
299 dynamic of the fluorescence decay observed in control cultures, indicates the presence of  
300 physiological bleaching of fluorophore over the acquisition time course, however s-GO and  
301 bzATP groups, despite the same bleaching-induced loss of fluorescence, showed a faster de-  
302 staining rate in respect to controls. This is also visualized by the time-lapse images framed at  
303 time 0 s, 300 s and 600 s of the crude recordings (Figure 1e middle and right panels). We  
304 quantified the fluorescence decay time constant ( $\tau$ ) values (box plot of Figure 1f) and detected  
305 shorter decay values in both bzATP and s-GO groups ( $\text{median}_{\text{control}}= 219$  s;  $\text{median}_{\text{bzATP}}= 184.2$   
306 s;  $\text{median}_{\text{s-GO}}= 163.9$  s). This result suggested that the membrane de-staining was actually related  
307 to MVs release, as expected in bzATP treated cells, more than to other membrane turnover  
308 activities. Such a release was comparable between bzATP and s-GO, both significantly faster  
309 than controls ( $P_{\text{bzATP}} < 0.001$ ;  $P_{\text{s-GO}} < 0.001$ ).



311 **Fig. 1. Graphene oxide nanosheets does not affect astrocytes vitality.** Cultured astrocytes release microvesicles  
 312 (MVs) upon ATP or s-GO stimulation. a) Confocal images visualize cultured astrocytes in control and after s-GO  
 313 (10  $\mu\text{g}/\text{mL}$ ; 6 days) treatment; anti-GFAP, in green, and DAPI (to visualize nuclei), in blue; scale bar 50  $\mu\text{m}$ . b) Box  
 314 plot summarizes the cell density measures; note the similar values in both groups. c) Confocal images visualize  
 315 cultured astrocytes in control and after s-GO (10  $\mu\text{g}/\text{mL}$ ; 6 days) treatment. Cultures were treated with propidium  
 316 iodide (PI) to visualize death cells. Anti-GFAP, in green, DAPI (to visualize nuclei), in blue and PI in red; scale bar  
 317 50  $\mu\text{m}$ . d) Histogram summarizes the percentage of death cells followed the s-GO exposure and in control condition;  
 318 note that there are no significant difference between two groups e) Surface membrane staining and activity  
 319 dependent de-staining of FM1-43 in cultured astrocytes, scale bar 25  $\mu\text{m}$ . f) Normalized FM1-43 de-staining traces  
 320 (top) in control astrocytes (light grey), in bzATP treated once (orange) and in s-GO treated once (black). The box  
 321 plot (bottom) summarizes the decay time constant  $\tau$  of FM1-43 de-staining in the three conditions (median<sub>control</sub> =  
 322 219.2 s; median<sub>bzATP</sub> = 184.2 s; median<sub>s-GO</sub> = 163.9 s). Thick horizontal bars in the box plots indicate median value;  
 323 boxed area extends from the 25<sup>th</sup> to 75<sup>th</sup> percentiles, whiskers from 2.5<sup>th</sup> to the 97.5<sup>th</sup> percentiles. Significance: \*\*P <  
 324 0.01 \*\*\*P < 0.001, Kruskal-Wallis test, Dunn's post hoc test).

326 The release of MVs suggested by FM1-43 measures, was confirmed by immunoblot analysis  
 327 for the biomarker flotillin-1 of the supernatant collected from control and treated cultures (Fig.  
 328 2a). As expected, bzATP stimulation and s-GO incubation induced the appearance of a thick  
 329 band corresponding to flotillin-1 (Figure 2a), a signature of MVs release by astrocytes, with an  
 330 additive effect between s-GO exposure and pharmacological stimulation with bzATP (s-GO<sub>Ringer</sub>  
 331 is quantified as 100 % more than Control<sub>Ringer</sub>; bzATP<sub>Ringer</sub> is quantified as 360 % more than  
 332 Control<sub>Ringer</sub>; bzATP<sub>s-GO</sub> is quantified as 2900 % more than Control<sub>Ringer</sub>. Calculated over three  
 333 independent experiments).[19,30,34] In control conditions only a weak band was perceived,  
 334 indicating that MVs constitutive release in culture was poorly detectable. Atomic force  
 335 microscopy (AFM) topographic reconstruction of re-suspended MVs pellet (Fig. 2b) confirmed  
 336 the presence of MVs detected by the immunoblot in both bzATP (mvA) and s-GO (mvG)  
 337 groups. When investigating the effect of shorter (3 days) exposure to s-GO, western blot  
 338 experiments (supplementary Fig. S2) showed the absence of a significant increase in MVs  
 339 constitutive release when compared to control. Yet, bzATP release of MVs was potentiated by 3

340 days s-GO (supplementary Fig. S2) suggesting that s-GO already modulated MVs release, but  
341 longer time of s-GO exposure are needed to enhance basal release in the absence of additional  
342 stimuli. In an additional set of western blot experiments, we tested the sensitivity of bzATP and  
343 s-GO MVs release to extracellular calcium deprivation (supplementary Fig. S3). Differently  
344 from bzATP, s-GO release was apparently not affected by calcium removal. In control condition,  
345 a thick band appeared upon calcium removal, suggestive of an increase in constitutive release  
346 (supplementary Fig. S3). These preliminary results hint at release mechanisms differently tuned  
347 by calcium among control, bzATP and s-GO and require further studies.

348 We systematically investigated and compared the MV size distribution by means of AFM and  
349 nanoparticle tracking analysis (NTA) measurements. AFM images show the presence of  
350 roundish protrusions of dimensions compatible with the size of MVs. No other kind of  
351 contaminant was present, to indicate that the procedure for isolating and collecting MVs from the  
352 medium was clean and effective. When analyzed by AFM (Fig. 2c) s-GO-derived MVs (mvG)  
353 lateral size were significantly smaller ( $n = 72$ ,  $\text{median}_{\text{mvG}} = 244 \text{ nm}$ ) than bzATP-derived ones  
354 (mvA;  $n = 107$ ,  $\text{median}_{\text{mvA}} = 479 \text{ nm}$ ) ( $P < 0.001$ ). Conversely, we detected no differences in MV  
355 height values ( $\text{median}_{\text{mvG}} = 19 \text{ nm}$ ;  $\text{median}_{\text{mvA}} = 22 \text{ nm}$ ;  $P = 0.17$ ). Within each group, the  
356 distribution of size values detected was not negatively correlated to the height, as shown in  
357 Figure 2d (left;  $r_{\text{mvG}} = 0.8808$  and  $r_{\text{mvA}} = 0.4039$ ;  $P < 0.001$ ). However, AFM experiments were  
358 performed in air, thus a not specific flattening of MVs caused by vesicle collapsing might have  
359 influenced these measurements. In principle differences in MV elastic properties, potentially  
360 related to diverse membrane components, might lead to a variable collapsing of MVs when  
361 measured in air.

362 Since AFM measurements are affected by the reduced size of the analyzed samples, and might  
363 not reflect the entire MVs population, we decided to use nanoparticle tracking analysis (NTA) to  
364 perform bulk analysis of vesicles in aqueous suspension. NTA tracks single particle Brownian  
365 motion within a dark field microscope, derives mean square vesicles velocity and translates them  
366 into size distribution.[35] NTA revealed a more complex pattern of size distribution (Fig. 2e): in  
367 the case of mvA we observed three subpopulations of vesicles at 115 nm, 235 nm and 400 nm  
368 respectively while in the case of mvG we found two partially overlapping peaks at 135 nm and  
369 168 nm, plus two distinct peaks at 275 nm and 385 nm (Fig. 2e). The diameter analysis revealed  
370 a slight, but not significant, difference between the two populations with the diameter of mvG  
371 smaller and less distributed, compared to those of mvA ( $\text{median}_{\text{mvA}} = 235.4 \text{ nm}$ ;  $\text{median}_{\text{mvG}} =$   
372  $183.6 \text{ nm}$ ) (Fig. 2f). These results convincingly suggested a comparable size distribution in both  
373 MV populations and subpopulations. However, we detected a significant difference in the  
374 number of vesicles released within the same time window (Fig. 2e) to indicate that cultures  
375 treated with s-GO produced more MVs when compared to cultures stimulated with bzATP (mvA  
376  $= \sim 3.32 \times 10^8 \text{ vesicle/mL}$ ; mvG  $= \sim 8.19 \times 10^8 \text{ vesicles/mL}$ ), consistently with our results obtained  
377 by MV release analysis and immunoblot (but see also Visnovitz et al. 2019[36]). Therefore, even  
378 though the overall size of the MV population produced did not change, s-GO was more efficient  
379 in generating MVs from astrocytes.



385 stimulated (bzATP) by 100  $\mu\text{M}$  bzATP. s-GO<sub>Ringer</sub> is quantified as 100% more than Control<sub>Ringer</sub>; bzATP<sub>Ringer</sub> is  
386 quantified as 360% more than Control<sub>Ringer</sub>; bzATP<sub>s-GO</sub> is quantified as 2900% more than Control<sub>Ringer</sub>. Calculated  
387 over three independent experiments. b) AFM topographic reconstruction of MVs isolated from cultured primary  
388 astrocytes treated with bzATP (100  $\mu\text{M}$ ) and s-GO (10  $\mu\text{g}/\text{mL}$ ) and performed in air (semi-contact mode). Scale bar  
389 500 nm. c) Lateral size values distribution and median values for both groups, note that mvG lateral size is  
390 significantly smaller than that of mvA (median<sub>mvA</sub> = 479 nm; median<sub>mvG</sub> = 244.1 nm; \*\*\*P > 0.001, Mann-Whitney  
391 test). d) AFM measures of lateral size are plotted against AFM measures of height of MVs isolated from glial cells  
392 treated by bzATP (100  $\mu\text{M}$ ; mvA; in orange) or by s-GO (10  $\mu\text{g}/\text{mL}$ ; mvG; in black). e) Size distribution of MVs  
393 isolated from glial cells treated by bzATP (100  $\mu\text{M}$ ; in orange) or by s-GO (10  $\mu\text{g}/\text{mL}$ ; in black) measured by  
394 nanoparticle tracking analysis (NTA). Values of the peaks are expressed in nm. f) Lateral size values distribution  
395 and median values for both groups, obtained by NTA measurement.

396

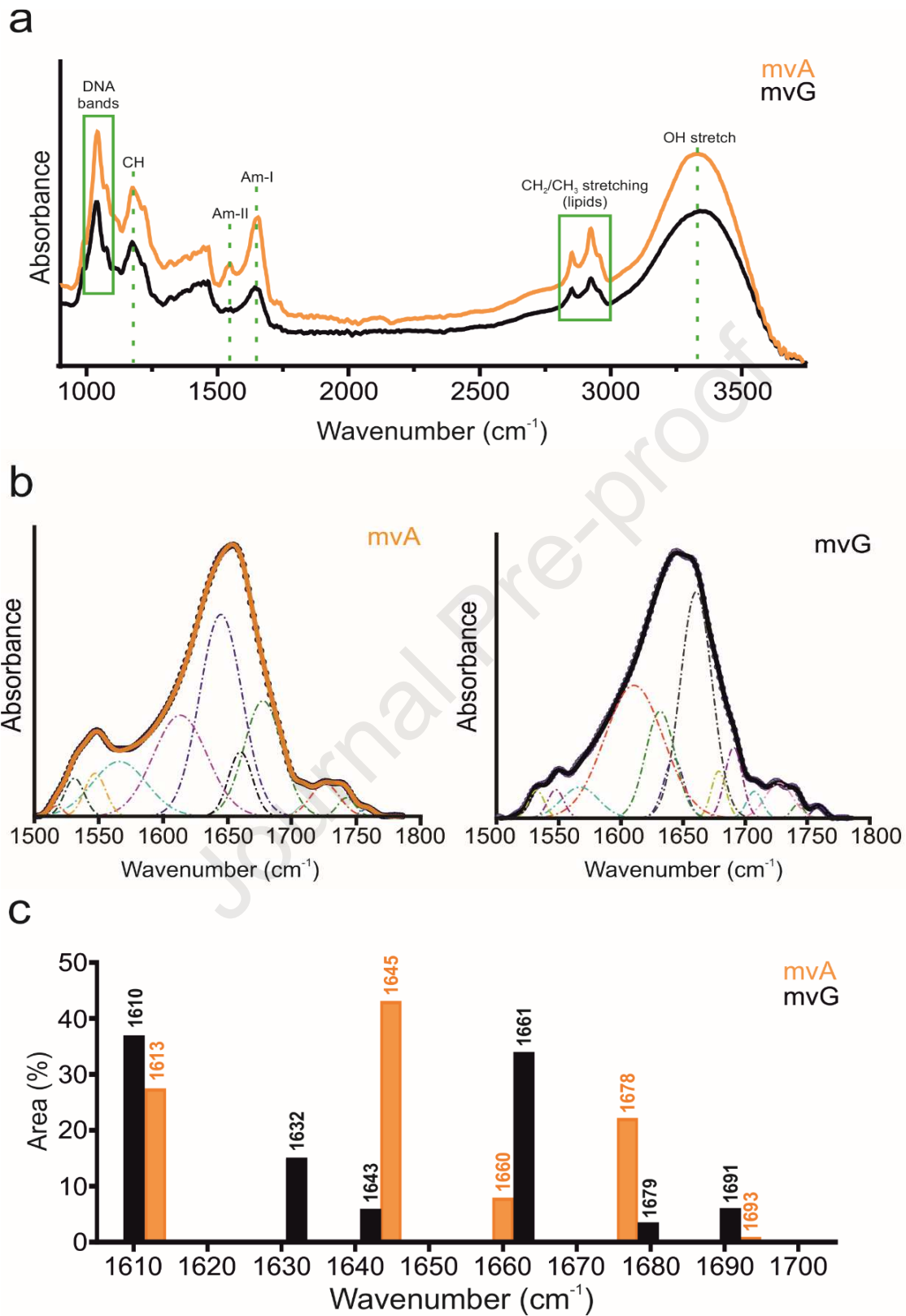
397

398 In order to analyze the macromolecular composition of MVs we took advantage of two  
399 complementary techniques: FTIR-ATR and UVRR spectroscopy. For these measurements, MVs  
400 were isolated by differential centrifugation as described before (see Material and Methods). To  
401 avoid any spurious effect due to the absorption of phosphate groups from the buffer, we washed  
402 and re-suspended the MVs pellet with a NaCl solution (150 mM). The infrared (IR) absorbance  
403 spectra (Fig. 3a) revealed a clear contribution of the CH and the phosphate bands linked to DNA  
404 in both samples, mvA and mvG, as well as the lipid signatures at 2900-3000  $\text{cm}^{-1}$ , arisen from  
405 the CH<sub>2</sub> and CH<sub>3</sub> stretching mode. The amide I and amide II bands between 1500 and 1785  $\text{cm}^{-1}$ ,  
406 the two major protein bands in the IR spectrum, show more pronounced differences between the  
407 two populations of vesicles. The amide I band, which is primarily related to the C=O stretching  
408 in the peptide bonds and modulated by the proteins' secondary structures, displayed similar  
409 shapes for mvA and mvG. The amide II band, primarily due to C-N stretching and N-H in plane  
410 bending vibrations, also reflecting the protein secondary structure, was instead clearly depleted  
411 in the case of mvG. To gain insights into the contribution of different protein secondary  
412 structures in the two families of vesicles, we analyzed the second derivative of the IR signal in

413 the amide I + amide II region (Fig. 3b) and used the position of the minima to guide a  
414 multicomponent gaussian fit of the bands in the region 1500 and 1785  $\text{cm}^{-1}$ . The % area  
415 contributions obtained by the fit are reported in Fig. 3c. The low-energy flank of amide I of both  
416 mvA and mvG is characterized by the presence of the 1610-1613  $\text{cm}^{-1}$  vibrational peak which  
417 could be addressed to a mixed contribution arisen from  $\beta$ -sheets and side-chains vibrations.  
418 Additionally, the band at 1660  $\text{cm}^{-1}$  might also be derived from the presence of RNA in the  
419 vesicles.[37] Noteworthy, the relative populations of the peaks at approximately 1645  $\text{cm}^{-1}$ ,  
420 1660  $\text{cm}^{-1}$  and 1678  $\text{cm}^{-1}$  are inverted between mvA and mvG. According to the literature[37],  
421 the 1645  $\text{cm}^{-1}$  peak (depleted in mvG) might be assigned to random structures and/or helices; the  
422 1660  $\text{cm}^{-1}$  peak (depleted in mvA) to flexible helices (as  $3_{10}$  helices); the 1678  $\text{cm}^{-1}$  peak  
423 (depleted in mvG) to beta structures such as b-turns. The bands at 1632  $\text{cm}^{-1}$  and at 1693  $\text{cm}^{-1}$ ,  
424 both present in the mvG only, are ascribed to anti-parallel beta sheet, as found in aggregates in  
425 tissues.[37,38] We can conclude that mvGs contain proteins with perturbed secondary structure,  
426 characterized by beta structure-based aggregates and flexible helices. No significant variations in  
427 the DNA phosphate bands were measured as well as the nature or localization of the DNA  
428 signature detected. It is interesting to note that in previous measures the DNA delivered by EVs  
429 has been reported to be stocked either inside the vesicles or on their surface[39].

430 UV Resonant Raman (UVRR) measurements taken using an excitation wavelength of 244 nm  
431 (see experimental section and supplementary Fig. S4) confirmed the amide I signal depression in  
432 mvG absorption spectrum. Due to an overlap between the UVRR s-GO band, we could not  
433 confirm or discard the presence of s-GO inside the vesicles. Thus, we cannot exclude that the  
434 changes in protein native structure might be due to s-GO altering the MV  
435 micro(nano)environment or the possibility of a general interference with the measurements. The

436 absence of astrocytes cytotoxicity, even upon prolonged exposure to s-GO, together with the  
437 functional measures of increased MVs release kinetic obtained by live imaging, are against a  
438 mere alteration in protein integrity due to denaturation of membrane proteins in the presence of  
439 s-GO.[40–42] FTIR-ATR spectroscopy is a powerful tool to assess the disordered character of  
440 proteins, and the absence of a well-defined structure under native conditions is a peculiar  
441 property of intrinsically disordered proteins (IDP).[43,44] In this framework, IDPs might  
442 represent a specific signal vehiculated by mvG and the lack of protein structural constraints  
443 could facilitate several, yet unknown, biological processes.[44]



445 **Fig. 3. MVs characterization by infrared spectroscopy.** Microvesicles produced by glial cells *via* bzATP or s-GO  
446 stimulation and characterized by infrared spectroscopy. a) Infrared spectra of microvesicles obtained by bzATP  
447 stimulation (mvA, in orange) or by s-GO exposure (mvG, in black) in the region 950-3600  $\text{cm}^{-1}$ . Contributions  
448 arisen from nucleic acids, proteins and lipids characterize the spectra. The two boxes in green and the green dashed  
449 lines are used as eye-guides to highlight nucleic acids,  $\text{CH}_2\text{-CH}_3$  stretching of lipids and protein amide bands,  
450 respectively. b) Fitting procedure applied to mvA (on the left) and mvG (on the right) amide bands spectra.  
451 Multicomponent Gaussian curves were used to actually reproduce the experimental data. The centres of the  
452 Gaussian curves were chosen as the minimum of the 2<sup>nd</sup> derivative of the spectrum and kept free to vary within 4  
453  $\text{cm}^{-1}$  around its maximum. c) Histograms representing the areas of the Gaussian curves used to reproduce the  
454 experimental data of mvA (in orange) and mvG (in black) in the region 1500-1785  $\text{cm}^{-1}$ . The areas of each band has  
455 been weighted respect to the total amide band area which they belongs to (i.e. 1640  $\text{cm}^{-1}$  band has been weighted  
456 with respect to the total Am-I band area).

457 It is clearly visible that mvA and mvG vesicles have a different secondary structure: the former is mainly  
458 characterized by an intense peak at 1645  $\text{cm}^{-1}$  (43%), which can be assigned to random structures/a-helix structure,  
459 and at 1678  $\text{cm}^{-1}$  (22%) usually assigned to b-turn and at 1613  $\text{cm}^{-1}$  (27%), which could be assigned to side chains  
460 vibrations; in contrast, mvG are mainly characterized by anti-parallel b-sheets structure (1632 (15%) and 1693  $\text{cm}^{-1}$   
461 (3%) bands) with a strong contribution of flexible 3-10 helix (1661  $\text{cm}^{-1}$  peak (34%)) and of side chain band at 1610  
462  $\text{cm}^{-1}$  (37%).

463

464 Finally, we set up a functional test to compare the impact of mvG delivery with that of mvA on  
465 synaptic activity, when neuronal networks are acutely and transiently exposed to MVs. To this  
466 aim, we isolated cortical neurons and glial cells from postnatal rat cortices and cultured them for  
467 10 days. Fig. 4a shows confocal high magnification microscopy images of cortical cultures  
468 where neurons were visualized by labeling class III  $\beta$ -tubulin (in red), a microtubule component  
469 expressed exclusively by neurons, while astrocytes were visualized by GFAP labeling (in  
470 green).[45] We patch-clamped visually identified cortical neurons (in voltage clamp  
471 configuration, holding potential – 70 mV), while a second pipette for the local delivery of saline  
472 solution was positioned at a distance of 200  $\mu\text{m}$  (under microscopy visual control) from the  
473 recorded cell (sketched in Fig. 4a, right). We estimated that, at this distance, the application of a  
474 brief (500 ms) pulse of pressure should result in a local (i.e. on the recorded neuron) and

475 transient delivery of standard saline solution alone or containing mvG or mvA (re-suspended in  
476 saline). A typical feature of these cultures is the prominent expression of spontaneous synaptic  
477 activity, represented by heterogeneous postsynaptic currents (PSCs) of variable frequency and  
478 amplitude (box plots in Fig. 4b). Baseline PSCs were recorded before (10 min) and after (15  
479 min) the local saline, mvG or mvA ejection. Fig. 4c shows representative current tracings where  
480 standard saline was pressure ejected (light grey, top), or where mvA solution (orange, middle)  
481 and mvG (black, bottom) were administered.

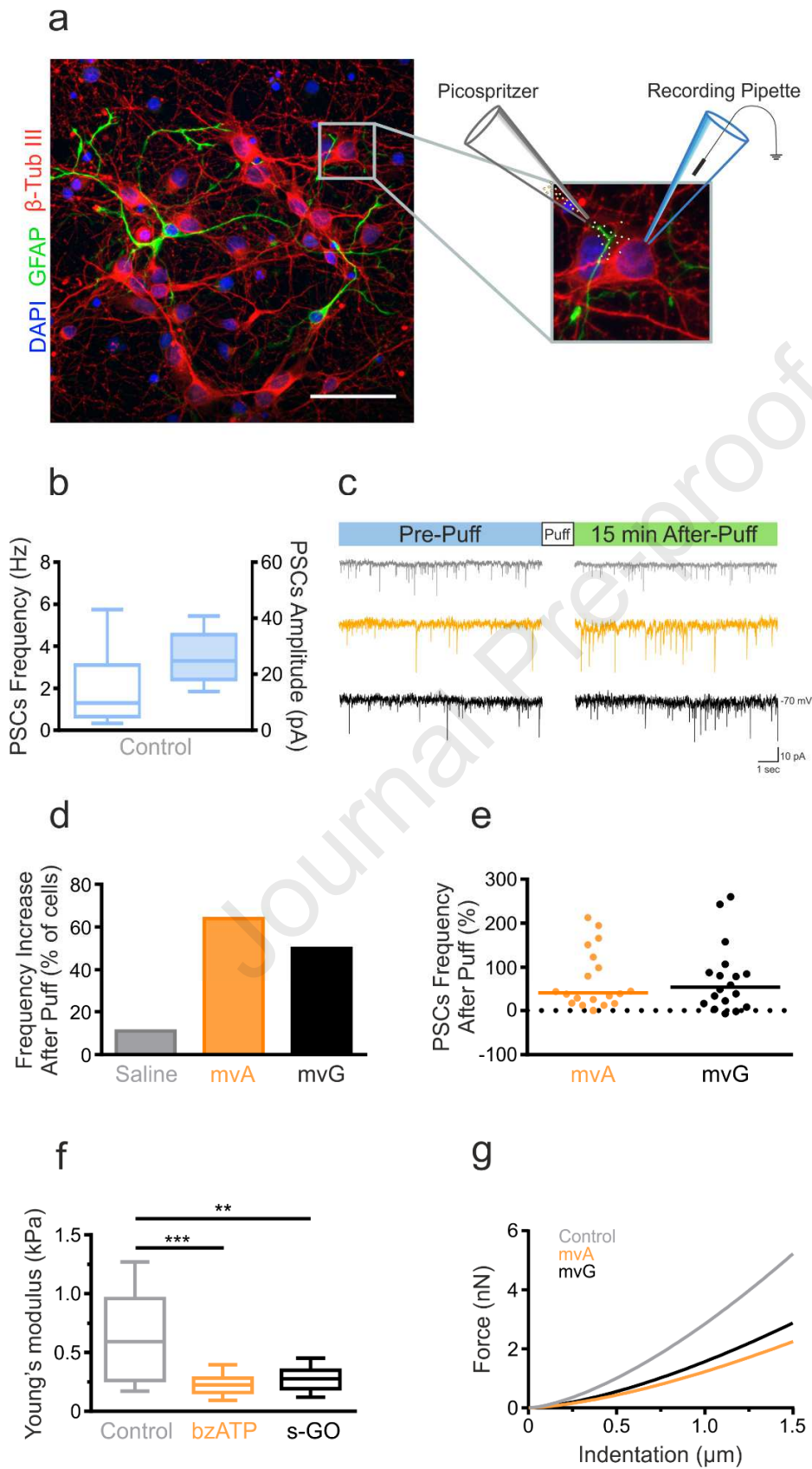
482 Since spontaneous fluctuations in PSCs frequency  $\leq 15\%$  of baseline values were frequently  
483 detected, we took this as the threshold value to estimate changes when comparing PSCs before  
484 and after pressure ejections of saline. In the large majority (88 %, n = 16/18 neurons; histograms  
485 in Fig. 4d) of neurons exposed to saline solution alone, spontaneous PSCs frequency did not  
486 change. On the contrary, within 5-8 min from the acute mvA and mvG ejections, PSCs frequency  
487 was stably increased in 64 % (n= 16/25 neurons, mvA) and 54 % (n= 13/24 neurons, mvG;  
488 summarized in the histograms of Fig. 4d) of recorded neurons. Fig. 4e shows the increases in  
489 PSCs frequency in individual experiments and highlights the variability of such changes when  
490 administering MVs, with increased frequencies ranging from 25 % to 200 %. Since we could not  
491 experimentally control the amount of MVs collected by primary astrocytes and delivered by  
492 pressure ejection, neurons were exposed to different amounts of MVs and this can in part explain  
493 the detected variability. PSCs frequency increases due to MVs exposures were not reversible  
494 upon 20 min washout. From such functional investigation, glial-signaling generated by ATP or s-  
495 GO affected similarly neuronal synapses upon transient, direct exposure.

496 To our knowledge, this is the first time that the functional effects of MVs generated by  
497 astrocytes on synaptic activity upon local delivery have been electrophysiologically documented.

498 Neuroglia extracellular vesicles have been described to provide support on synaptic activity, with  
499 the majority of studies focused on microglia and inflammation, apparently regulating neural  
500 transmission at the pre-synaptic level.[5,46–48] Astrocytic MVs have been proposed to exert  
501 neuroprotective effects in neuropathology and in physiology, however the role of astrocytes or of  
502 discrete astrocyte populations in delivering different messages via MV release has yet to be  
503 elucidated.[49,50]

504 After assessment of the ability of MVs released by glial cells to affect cortical neuron  
505 physiology within min after their interaction with the targeted neuron, we asked if the presumed  
506 fusion of vesicles with neuronal plasma membrane could also affect their mechanical properties.  
507 To investigate this aspect, we delivered MVs obtained from glial cultures previously treated with  
508 bzATP or s-GO to cortical neurons by re-suspending the isolated MVs in 100  $\mu$ L of neuronal  
509 culture medium and adding them to neuronal cultures. 24 hours after the exposure, force  
510 spectroscopy measurement on treated neuronal cultures were performed with AFM by  
511 positioning the tipless cantilever with a borosilicate glass bead previously glued on it[51], at the  
512 center of randomly chosen neurons. As showed by the boxplot in Fig. 4f, the exposure to mvA  
513 caused a significant softening of neuronal soma, when compared to controls ( $\text{median}_{\text{mvA}} = 0.22$   
514 kPa,  $\text{median}_{\text{control}} = 0.59$  kPa;  $P_{\text{mvA}} < 0.001$ ). A similar result was observed also in the case of  
515 mvG exposure even if the effect exerted on neuronal stiffness is less pronounced than that  
516 induced by mvA ( $\text{median}_{\text{mvG}} = 0.28$  kPa,  $\text{median}_{\text{control}} = 0.59$  kPa;  $P_{\text{mvG}} < 0.01$ ). The reported  
517 effect of mvA and mvG on neuronal cell mechanical properties is presumably a consequence of  
518 vesicular fusion with the cellular plasma membrane, which may affect its lipid composition.  
519 Since the mechanical properties of a cell are mostly defined by plasma membrane features and  
520 the ones of the underlying cytoskeleton, a change in neuronal plasma membrane lipid

521 composition can partially justify the observed reduction in mvA and mvG-treated neurons  
522 stiffness.[52] In particular, glia-derived MVs are able to transport the enzyme Acid  
523 sphingomyelinase (A-SMase) involved in the metabolism of sphingomyelin (SM), a precursor of  
524 the phospholipid sphingosine (sph). Sph and its metabolites have been already reported to play a  
525 fundamental role in facilitating synaptic vesicles release by changing the membrane composition  
526 at pre-synaptic level.[48,53] This intrinsic capacity of MVs to participate in membrane lipid  
527 metabolism may therefore modulate the contribution of plasma membrane to neuronal rigidity.  
528 In this context, the slight difference of stiffness values reported among mvA and mvG-treated  
529 neurons, although not statistically significant ( $P_{mvA-mvG} > 0.05$ ) should not be  
530 underestimated.[54,55] It is tempting to speculate that this difference can be explained by the  
531 presence of specific proteins in the vesicles, that are unstable in mvG. Based on our measures,  
532 we cannot exclude the presence of residual s-GO flakes either inside or on the vesicle surface. It  
533 is known that GO is reportedly able to interact with the hydrophobic region of biological and  
534 model lipid membranes, even though the nature of the interaction is strictly dependent to its size  
535 and degree of surface oxygenation.[56,57] Assuming that the GO nanosheets, once added to the  
536 culture medium, can adsorb on plasma membrane or pierce it and being embedded in the lipid  
537 bilayer, there is a concrete possibility that MVs, which directly originate from plasma membrane,  
538 can include those flakes in their structure.[30] The horizontal transfer of s-GO from glial cells to  
539 cortical neurons, mediated by MVs, may therefore affect plasma membrane rigidity of targeted  
540 neurons. Regardless of this, we can exclude a direct effect of s-GO in synaptic transmission,  
541 reported to be transient and reversible upon acute exposure, in view of the persistent modulation  
542 of synaptic current frequency brought about by MVs.[19,20]



543

544 **Fig. 4. MVs released by astrocytes affect cortical neuron post-synaptic activity and mechanical properties.**  
 545 Potentiation of synaptic activity upon local applications of MVs in cortical neurons. a) Confocal micrograph  
 546 visualizing cortical primary cultures at 8 days in vitro; anti-class III  $\beta$ -tubulin is used to visualize neurons (in red),  
 547 anti-GFAP for astrocytes (in green) and DAPI (in blue) to visualize neurons. Scale bar 50  $\mu$ m. On the right, a  
 548 representation of the experimental setting for the simultaneous MVs pressure-release (*puff*) and the cell patch-clamp  
 549 recording from cultured neurons. b) Box plot summarizes the PSCs frequency and amplitude values in control  
 550 cortical neurons. c) Top: diagram of the experimental protocol. Bottom: representative current tracings of the  
 551 spontaneous synaptic activity detected prior and after puff applications of control saline (in light grey) or mvA (in  
 552 orange) or mvG (in black). d) Bar plots of pooled data summarize the % of cells displaying PSCs frequency increase  
 553 upon delivery of pressure ejected saline (light grey), mvA (orange) and mvG (black). Note that in control (saline)  
 554 the large majority (88 %) of neurons did not increase their basal activity. e) The plot summarizes the distribution of  
 555 the % of increase in PCSs frequency detected within the three groups. f) Elastic moduli of cortical neurons, grown  
 556 on glass, and exposed to MVs isolated from glial cells previously treated with bzATP (orange) or s-GO flakes  
 557 (black). Neurons treated with mvA and mvG are significantly less rigid if compared with control ( $P_{mvA} < 0.001$ ;  
 558  $P_{mvG} < 0.01$ ). Thick horizontal bars in the box plots indicate median value; boxed area extends from the 25<sup>th</sup> to 75<sup>th</sup>  
 559 percentiles, whiskers from 5<sup>th</sup> to the 95<sup>th</sup> percentiles. Significance: \*\*P < 0.01 \*\*\*P < 0.001, Kruskal-Wallis test,  
 560 Dunn's post hoc test) g. Indentation curves of cortical neurons previously treated with mvA or mvG.  
 561

#### 562 4. Conclusion

563 Astrocyte-derived MVs may play significant roles in propagating signaling molecules, in CNS  
 564 physiology and disease. Despite the increasing knowledge on extracellular vesicles (in particular  
 565 exosomes) ability to promote inflammation or contribute in spreading of pathogenic proteins in  
 566 neurodegenerative disorders (from Amyotrophic Lateral Sclerosis to Alzheimer disease [58,59])  
 567 little is currently known on their properties (mechanical, biochemical, lipid membrane  
 568 composition, cargo nature etc.), in particular when focusing on the smaller class of such natural  
 569 vectors, the MVs. Nevertheless, MVs emerge as key players in neuronal and synaptic  
 570 physiology, able to influence neurotransmission, or to support neurons.[48,60–62] In our study,  
 571 we report the ability of artificially generating MVs by s-GO transient exposure. MVs generated  
 572 by s-GO were apparently characterized by altered protein content when compared to the ATP-  
 573 driven ones. Intriguingly, the tuning of synaptic activity by mvG or mvA was similar,

574 supposedly being related to features diverse from MV protein content. The ability of s-GO to  
575 interfere with exo-endocytotic membrane dynamics is not surprising, indeed we have described  
576 the ability of s-GO nanoflakes to interfere with presynaptic vesicle release *in vitro* and *in*  
577 *vivo*. [19,20] In the current work, we describe the direct interference of MVs with synaptic  
578 activity, presumably due to MVs fusion with the target neuron plasma membrane. Such an  
579 approach holds the potential to open new opportunities in engineering MVs for synaptic  
580 targeting. In this framework, it is tempting to speculate that s-GO interactions with the cell  
581 membrane mimic extracellular mechanical signaling at the nanoscale sufficient to enable the  
582 release of MVs, thus representing unconventional tools to exploit the physics governing vesicle  
583 release. We feel pertinent here to consider the fact, that the enormous potentiality of graphene-  
584 based materials in nanomedicine has already promoted the development of new generation-  
585 nanocarriers for either gene or drug delivery [17,63]. In this framework, we may speculate on  
586 future developments where engineered cells are mechanically induced to release MVs, carrying  
587 GO nanoflakes properly functionalized to deliver genes or drugs of interest and thus representing  
588 either the trigger and the cargo.

589

590 ASSOCIATED CONTENT

591 **Supporting Information**

592 Supporting experimental section

593 Supporting results, Figures S1–S4 and Table S1.

594 AUTHOR INFORMATION

595 **Corresponding Author**

596 \*E-mail: laura.ballerini@sissa.it

597 \*E-mail: loredana.casalis@elettra.eu

## 598 **Present Addresses**

599 <sup>†</sup>Center for Synaptic Neuroscience, Istituto Italiano di Tecnologia (IIT), 16132, Genoa, Italy

## 600 **Author Contributions**

601 M.M. performed cell biology, electrophysiology, and immunofluorescence experiments and  
602 analysis; M.M. and P.P. designed and performed AFM experiments; M.P. performed IR and  
603 UVRR experiments and analysis. CM and GDM performed biology and WB experiments; N.L.  
604 and K.K. contributed to the synthesis and characterization of thin graphene oxide of biological  
605 grade. BB performed SEM micrographs of GO. L.B. and L.C. conceived the study; L.B.  
606 conceived the experimental design and contributed to the analysis of data; L.B. wrote the  
607 manuscript.

## 608 **Notes**

609 The authors declare no competing financial interest.

610

## 611 **ACKNOWLEDGMENT**

612 We acknowledge the financial support from the European Union's Horizon 2020 Research and  
613 Innovation Programme under grant agreement no. 785219 and no. 881603 Graphene Flagship.  
614 MM, PP and LC acknowledge CERIC-ERIC proposal grant n. 20167063 for the IR  
615 measurements, performed at the SISSI-Bio beamline of Elettra Sincrotrone Trieste. PP and LC

616 acknowledge also the European Regional Development Fund and Interreg V-A Italia-Austria  
617 2014-2020 project EXOTHERA (ITAT1036).

## 618 REFERENCES

- 619 [1] D.A. Shifrin, M.D. Beckler, R.J. Coffey, M.J. Tyska, Extracellular vesicles:  
620 communication, coercion, and conditioning, *Mol. Biol. Cell.* 24 (2013) 1253–1259.  
621 <https://doi.org/10.1091/mbc.e12-08-0572>.
- 622 [2] Y.J. Yoon, O.Y. Kim, Y.S. Gho, Extracellular vesicles as emerging intercellular  
623 comunicasomes., *BMB Rep.* 47 (2014) 531–9.  
624 <https://doi.org/10.5483/BMBREP.2014.47.10.164>.
- 625 [3] V. Zappulli, K.P. Friis, Z. Fitzpatrick, C.A. Maguire, X.O. Breakefield, Extracellular  
626 vesicles and intercellular communication within the nervous system, *J. Clin. Invest.* 126  
627 (2016) 1198–1207. <https://doi.org/10.1172/JCI81134>.
- 628 [4] C.P.-K. Lai, X.O. Breakefield, Role of Exosomes/Microvesicles in the Nervous System  
629 and Use in Emerging Therapies, *Front. Physiol.* 3 (2012) 228.  
630 <https://doi.org/10.3389/fphys.2012.00228>.
- 631 [5] V. Budnik, C. Ruiz-Cañada, F. Wendler, Extracellular vesicles round off communication  
632 in the nervous system., *Nat. Rev. Neurosci.* 17 (2016) 160–72.  
633 <https://doi.org/10.1038/nrn.2015.29>.
- 634 [6] A. Grimaldi, C. Serpe, G. Chece, V. Nigro, A. Sarra, B. Ruzicka, M. Relucenti, G.  
635 Familiari, G. Ruocco, G.R. Pascucci, F. Guerrieri, C. Limatola, M. Catalano, Microglia-  
636 Derived Microvesicles Affect Microglia Phenotype in Glioma, *Front. Cell. Neurosci.* 13

- 637 (2019) 41. <https://doi.org/10.3389/fncel.2019.00041>.
- 638 [7] E. Cocucci, J. Meldolesi, Ectosomes and exosomes: shedding the confusion between  
639 extracellular vesicles., *Trends Cell Biol.* 25 (2015) 364–72.  
640 <https://doi.org/10.1016/j.tcb.2015.01.004>.
- 641 [8] G. Raposo, W. Stoorvogel, Extracellular vesicles: exosomes, microvesicles, and friends.,  
642 *J. Cell Biol.* 200 (2013) 373–83. <https://doi.org/10.1083/jcb.201211138>.
- 643 [9] S.L.N. Maas, X.O. Breakefield, A.M. Weaver, Extracellular Vesicles: Unique Intercellular  
644 Delivery Vehicles, *Trends Cell Biol.* 27 (2017) 172–188.  
645 <https://doi.org/10.1016/j.tcb.2016.11.003>.
- 646 [10] C. Frühbeis, D. Fröhlich, E.-M. Krämer-Albers, Emerging Roles of Exosomes in Neuron–  
647 Glia Communication, *Front. Physiol.* 3 (2012) 119.  
648 <https://doi.org/10.3389/fphys.2012.00119>.
- 649 [11] G. Lachenal, K. Pernet-Gallay, M. Chivet, F.J. Hemming, A. Belly, G. Bodon, B. Blot, G.  
650 Haase, Y. Goldberg, R. Sadoul, Release of exosomes from differentiated neurons and its  
651 regulation by synaptic glutamatergic activity., *Mol. Cell. Neurosci.* 46 (2011) 409–18.  
652 <https://doi.org/10.1016/j.mcn.2010.11.004>.
- 653 [12] K.E. van der Vos, L. Balaj, J. Skog, X.O. Breakefield, Brain tumor microvesicles: insights  
654 into intercellular communication in the nervous system., *Cell. Mol. Neurobiol.* 31 (2011)  
655 949–59. <https://doi.org/10.1007/s10571-011-9697-y>.
- 656 [13] D. Ha, N. Yang, V. Nadiathe, Exosomes as therapeutic drug carriers and delivery vehicles  
657 across biological membranes: current perspectives and future challenges, *Acta Pharm. Sin.*

- 658 B. 6 (2016) 287–296. <https://doi.org/10.1016/J.APSB.2016.02.001>.
- 659 [14] C. Verderio, L. Muzio, E. Turola, A. Bergami, L. Novellino, F. Ruffini, L. Riganti, I.  
660 Corradini, M. Francolini, L. Garzetti, C. Maiorino, F. Servida, A. Vercelli, M. Rocca,  
661 D.D. Libera, V. Martinelli, G. Comi, G. Martino, M. Matteoli, R. Furlan, Myeloid  
662 microvesicles are a marker and therapeutic target for neuroinflammation, *Ann. Neurol.* 72  
663 (2012) 610–624. <https://doi.org/10.1002/ana.23627>.
- 664 [15] S. EL Andaloussi, I. Mäger, X.O. Breakefield, M.J.A. Wood, Extracellular vesicles:  
665 biology and emerging therapeutic opportunities, *Nat. Rev. Drug Discov.* 12 (2013) 347–  
666 357. <https://doi.org/10.1038/nrd3978>.
- 667 [16] K.P. Loh, Q. Bao, G. Eda, M. Chhowalla, Graphene oxide as a chemically tunable  
668 platform for optical applications, *Nat. Chem.* 2 (2010) 1015–1024.  
669 <https://doi.org/10.1038/nchem.907>.
- 670 [17] G. Reina, J.M. González-Domínguez, A. Criado, E. Vázquez, A. Bianco, M. Prato,  
671 Promises, facts and challenges for graphene in biomedical applications, *Chem. Soc. Rev.*  
672 46 (2017) 4400–4416. <https://doi.org/10.1039/c7cs00363c>.
- 673 [18] M. Baldrighi, M. Trusel, R. Tonini, S. Giordani, Carbon Nanomaterials Interfacing with  
674 Neurons: An In vivo Perspective, *Front. Neurosci.* 10 (2016) 250.  
675 <https://doi.org/10.3389/fnins.2016.00250>.
- 676 [19] R. Rauti, N. Lozano, V. León, D. Scaini, M. Musto, I. Rago, F.P. Ulloa Severino, A.  
677 Fabbro, L. Casalis, E. Vázquez, K. Kostarelos, M. Prato, L. Ballerini, Graphene Oxide  
678 Nanosheets Reshape Synaptic Function in Cultured Brain Networks, *ACS Nano.* 10

- 679 (2016) 4459–4471. <https://doi.org/10.1021/acsnano.6b00130>.
- 680 [20] R. Rauti, M. Medelin, L. Newman, S. Vranic, G. Reina, A. Bianco, M. Prato, K.  
681 Kostarelos, L. Ballerini, Graphene Oxide Flakes Tune Excitatory Neurotransmission in  
682 Vivo by Targeting Hippocampal Synapses, *Nano Lett.* 19 (2019) 2858–2870.  
683 <https://doi.org/10.1021/acs.nanolett.8b04903>.
- 684 [21] Z. Song, Y. Wang, Z. Xu, Mechanical responses of the bio-nano interface: A molecular  
685 dynamics study of graphene-coated lipid membrane, *Theor. Appl. Mech. Lett.* 5 (2015)  
686 231–235. <https://doi.org/10.1016/j.taml.2015.11.003>.
- 687 [22] R.J. Rodrigues, A.R. Tomé, R.A. Cunha, ATP as a multi-target danger signal in the brain,  
688 *Front. Neurosci.* 9 (2015) 148. <https://doi.org/10.3389/fnins.2015.00148>.
- 689 [23] F. Calegari, S. Coco, E. Taverna, M. Bassetti, C. Verderio, N. Corradi, M. Matteoli, P.  
690 Rosa, A regulated secretory pathway in cultured hippocampal astrocytes., *J. Biol. Chem.*  
691 274 (1999) 22539–47.
- 692 [24] P. Hermanowicz, M. Sarna, K. Burda, H. Gabryś, AtomicJ: An open source software for  
693 analysis of force curves, *Rev. Sci. Instrum.* 85 (2014) 063703.  
694 <https://doi.org/10.1063/1.4881683>.
- 695 [25] F. D’Amico, M. Saito, F. Bencivenga, M. Marsi, A. Gessini, G. Camisasca, E. Principi, R.  
696 Cucini, S. Di Fonzo, A. Battistoni, E. Giangrisostomi, C. Masciovecchio, UV resonant  
697 Raman scattering facility at Elettra, *Nucl. Instruments Methods Phys. Res. Sect. A Accel.*  
698 *Spectrometers, Detect. Assoc. Equip.* 703 (2013) 33–37.  
699 <https://doi.org/10.1016/J.NIMA.2012.11.037>.

- 700 [26] A. Bignami, L.F. Eng, D. Dahl, C.T. Uyeda, Localization of the glial fibrillary acidic  
701 protein in astrocytes by immunofluorescence, *Brain Res.* 43 (1972) 429–435.  
702 [https://doi.org/10.1016/0006-8993\(72\)90398-8](https://doi.org/10.1016/0006-8993(72)90398-8).
- 703 [27] M. Musto, R. Rauti, A.F. Rodrigues, E. Bonechi, C. Ballerini, K. Kostarelos, L. Ballerini,  
704 3D Organotypic Spinal Cultures: Exploring Neuron and Neuroglia Responses Upon  
705 Prolonged Exposure to Graphene Oxide, *Front. Syst. Neurosci.* 13 (2019) 1.  
706 <https://doi.org/10.3389/fnsys.2019.00001>.
- 707 [28] M. Bramini, G. Alberini, E. Colombo, M. Chiacchiaretta, M.L. DiFrancesco, J.F. Maya-  
708 Vetencourt, L. Maragliano, F. Benfenati, F. Cesca, Interfacing graphene-based materials  
709 with neural cells, *Front. Syst. Neurosci.* 12 (2018) 12.  
710 <https://doi.org/10.3389/fnsys.2018.00012>.
- 711 [29] A.B. Seabra, A.J. Paula, R. De Lima, O.L. Alves, N. Durán, Nanotoxicity of graphene and  
712 graphene oxide, *Chem. Res. Toxicol.* 27 (2014) 159–168.  
713 <https://doi.org/10.1021/tx400385x>.
- 714 [30] F. Bianco, C. Perrotta, L. Novellino, M. Francolini, L. Riganti, E. Menna, L. Saglietti,  
715 E.H. Schuchman, R. Furlan, E. Clementi, M. Matteoli, C. Verderio, Acid  
716 sphingomyelinase activity triggers microparticle release from glial cells, *EMBO J.* 28  
717 (2009) 1043–1054. <https://doi.org/10.1038/emboj.2009.45>.
- 718 [31] E. Amaral, S. Guatimosim, C. Guatimosim, Using the Fluorescent Styryl Dye FM1-43 to  
719 Visualize Synaptic Vesicles Exocytosis and Endocytosis in Motor Nerve Terminals, in:  
720 *Methods Mol. Biol.*, 2011: pp. 137–148. [https://doi.org/10.1007/978-1-60761-950-5\\_8](https://doi.org/10.1007/978-1-60761-950-5_8).

- 721 [32] W.J. Betz, F. Mao, C.B. Smith, Imaging exocytosis and endocytosis, *Curr. Opin.*  
722 *Neurobiol.* 6 (1996) 365–371. [https://doi.org/10.1016/S0959-4388\(96\)80121-8](https://doi.org/10.1016/S0959-4388(96)80121-8).
- 723 [33] A. Brumback, J.L. Lieber, J.K. Angleson, W.J. Betz, Using FM1-43 to study neuropeptide  
724 granule dynamics and exocytosis, *Methods.* 33 (2004) 287–294.  
725 <https://doi.org/10.1016/j.ymeth.2004.01.002>.
- 726 [34] Y. Yoshioka, Y. Konishi, N. Kosaka, T. Katsuda, T. Kato, T. Ochiya, Comparative  
727 marker analysis of extracellular vesicles in different human cancer types., *J. Extracell.*  
728 *Vesicles.* 2 (2013). <https://doi.org/10.3402/jev.v2i0.20424>.
- 729 [35] R.A. Dragovic, C. Gardiner, A.S. Brooks, D.S. Tannetta, D.J.P. Ferguson, P. Hole, B.  
730 Carr, C.W.G. Redman, A.L. Harris, P.J. Dobson, P. Harrison, I.L. Sargent, Sizing and  
731 phenotyping of cellular vesicles using Nanoparticle Tracking Analysis., *Nanomedicine.* 7  
732 (2011) 780–8. <https://doi.org/10.1016/j.nano.2011.04.003>.
- 733 [36] T. Visnovitz, X. Osteikoetxea, B.W. Sódar, J. Mihály, P. Lőrincz, K. V. Vukman, E.Á.  
734 Tóth, A. Koncz, I. Székács, R. Horváth, Z. Varga, E.I. Buzás, An improved 96 well plate  
735 format lipid quantification assay for standardisation of experiments with extracellular  
736 vesicles, *J. Extracell. Vesicles.* 8 (2019) 1565263.  
737 <https://doi.org/10.1080/20013078.2019.1565263>.
- 738 [37] J. Mihály, R. Deák, I.C. Szigyártó, A. Bóta, T. Beke-Somfai, Z. Varga, Characterization  
739 of extracellular vesicles by IR spectroscopy: Fast and simple classification based on amide  
740 and C H stretching vibrations, *Biochim. Biophys. Acta - Biomembr.* 1859 (2017) 459–  
741 466. <https://doi.org/10.1016/j.bbamem.2016.12.005>.

- 742 [38] D. Ami, F. Lavatelli, P. Rognoni, G. Palladini, S. Raimondi, S. Giorgetti, L. Monti, S.M.  
743 Doglia, A. Natalello, G. Merlini, In situ characterization of protein aggregates in human  
744 tissues affected by light chain amyloidosis: a FTIR microspectroscopy study, *Sci. Rep.* 6  
745 (2016) 29096. <https://doi.org/10.1038/srep29096>.
- 746 [39] A. Németh, N. Orgovan, B.W. Sódar, X. Osteikoetxea, K. Pálóczi, K. Szabó-Taylor, K. V.  
747 Vukman, Á. Kittel, L. Turiák, Z. Wiener, S. Tóth, L. Drahos, K. Vékey, R. Horvath, E.I.  
748 Buzás, Antibiotic-induced release of small extracellular vesicles (exosomes) with surface-  
749 associated DNA, *Sci. Rep.* 7 (2017) 1–16. <https://doi.org/10.1038/s41598-017-08392-1>.
- 750 [40] M.Y. Sherman, A.L. Goldberg, Cellular defenses against unfolded proteins: a cell  
751 biologist thinks about neurodegenerative diseases., *Neuron.* 29 (2001) 15–32.  
752 [https://doi.org/10.1016/s0896-6273\(01\)00177-5](https://doi.org/10.1016/s0896-6273(01)00177-5).
- 753 [41] R. V Rao, D.E. Bredesen, Misfolded proteins, endoplasmic reticulum stress and  
754 neurodegeneration., *Curr. Opin. Cell Biol.* 16 (2004) 653–62.  
755 <https://doi.org/10.1016/j.ceb.2004.09.012>.
- 756 [42] D.J. Selkoe, Folding proteins in fatal ways, *Nature.* 426 (2003) 900–904.  
757 <https://doi.org/10.1038/nature02264>.
- 758 [43] A. Natalello, D. Ami, S.M. Doglia, Fourier Transform Infrared Spectroscopy of  
759 Intrinsically Disordered Proteins: Measurement Procedures and Data Analyses, in:  
760 *Methods Mol. Biol.*, 2012: pp. 229–244. [https://doi.org/10.1007/978-1-61779-927-3\\_16](https://doi.org/10.1007/978-1-61779-927-3_16).
- 761 [44] C.J. Oldfield, A.K. Dunker, Intrinsically Disordered Proteins and Intrinsically Disordered  
762 Protein Regions, *Annu. Rev. Biochem.* 83 (2014) 553–584.

- 763 <https://doi.org/10.1146/annurev-biochem-072711-164947>.
- 764 [45] D. V Caccamo, M.M. Herman, A. Frankfurter, C.D. Katsetos, V.P. Collins, L.J.  
765 Rubinstein, An immunohistochemical study of neuropeptides and neuronal cytoskeletal  
766 proteins in the neuroepithelial component of a spontaneous murine ovarian teratoma.  
767 Primitive neuroepithelium displays immunoreactivity for neuropeptides and neuron-  
768 associated beta-tu, *Am. J. Pathol.* 135 (1989) 801–13.
- 769 [46] R.C. Paolicelli, G. Bergamini, L. Rajendran, Cell-to-cell Communication by Extracellular  
770 Vesicles: Focus on Microglia, *Neuroscience.* (2018).  
771 <https://doi.org/10.1016/j.neuroscience.2018.04.003>.
- 772 [47] Y. Yang, A. Boza-Serrano, C.J.R. Dunning, B.H. Clausen, K.L. Lambertsen, T.  
773 Deierborg, Inflammation leads to distinct populations of extracellular vesicles from  
774 microglia, *J. Neuroinflammation.* 15 (2018) 168. [https://doi.org/10.1186/s12974-018-](https://doi.org/10.1186/s12974-018-1204-7)  
775 [1204-7](https://doi.org/10.1186/s12974-018-1204-7).
- 776 [48] F. Antonucci, E. Turola, L. Riganti, M. Caleo, M. Gabrielli, C. Perrotta, L. Novellino, E.  
777 Clementi, P. Giussani, P. Viani, M. Matteoli, C. Verderio, Microvesicles released from  
778 microglia stimulate synaptic activity via enhanced sphingolipid metabolism, *EMBO J.* 31  
779 (2012) 1231–1240. <https://doi.org/10.1038/emboj.2011.489>.
- 780 [49] M.J. Carson, J.C. Thrash, B. Walter, The cellular response in neuroinflammation: The role  
781 of leukocytes, microglia and astrocytes in neuronal death and survival., *Clin. Neurosci.*  
782 *Res.* 6 (2006) 237–245. <https://doi.org/10.1016/j.cnr.2006.09.004>.
- 783 [50] M.M. Holm, J. Kaiser, M.E. Schwab, Extracellular Vesicles: Multimodal Envoys in

- 784 Neural Maintenance and Repair., *Trends Neurosci.* 41 (2018) 360–372.  
785 <https://doi.org/10.1016/j.tins.2018.03.006>.
- 786 [51] T. Gerecsei, I. Erdódi, B. Peter, C. Hós, S. Kurunczi, I. Derényi, B. Szabó, R. Horvath,  
787 Adhesion force measurements on functionalized microbeads: An in-depth comparison of  
788 computer controlled micropipette and fluidic force microscopy, *J. Colloid Interface Sci.*  
789 555 (2019) 245–253. <https://doi.org/10.1016/j.jcis.2019.07.102>.
- 790 [52] S. Kasas, X. Wang, H. Hirling, R. Marsault, B. Huni, A. Yersin, R. Regazzi, G.  
791 Grenningloh, B. Riederer, L. Forrò, G. Dietler, S. Catsicas, Superficial and deep changes  
792 of cellular mechanical properties following cytoskeleton disassembly, *Cell Motil.*  
793 *Cytoskeleton.* 62 (2005) 124–132. <https://doi.org/10.1002/cm.20086>.
- 794 [53] E. Norman, R.G. Cutler, R. Flannery, Y. Wang, M.P. Mattson, Plasma membrane  
795 sphingomyelin hydrolysis increases hippocampal neuron excitability by sphingosine-1-  
796 phosphate mediated mechanisms, *J. Neurochem.* 114 (2010) 430–439.  
797 <https://doi.org/10.1111/j.1471-4159.2010.06779.x>.
- 798 [54] V. Amrhein, S. Greenland, B. McShane, Scientists rise up against statistical significance,  
799 *Nature.* 567 (2019) 305–307. <https://doi.org/10.1038/d41586-019-00857-9>.
- 800 [55] It's time to talk about ditching statistical significance, *Nature.* 567 (2019) 283–283.  
801 <https://doi.org/10.1038/d41586-019-00874-8>.
- 802 [56] R. Frost, S. Svedhem, C. Langhammer, B. Kasemo, Graphene Oxide and Lipid  
803 Membranes: Size-Dependent Interactions, *Langmuir.* 32 (2016) 2708–2717.  
804 <https://doi.org/10.1021/acs.langmuir.5b03239>.

- 805 [57] N. Li, Q. Zhang, S. Gao, Q. Song, R. Huang, L. Wang, L. Liu, J. Dai, M. Tang, G. Cheng,  
806 Three-dimensional graphene foam as a biocompatible and conductive scaffold for neural  
807 stem cells, *Sci. Rep.* 3 (2013) 1604. <https://doi.org/10.1038/srep01604>.
- 808 [58] M. Basso, S. Pozzi, M. Tortarolo, F. Fiordaliso, C. Bisighini, L. Pasetto, G. Spaltro, D.  
809 Lidonnici, F. Gensano, E. Battaglia, C. Bendotti, V. Bonetto, Mutant copper-zinc  
810 superoxide dismutase (SOD1) induces protein secretion pathway alterations and exosome  
811 release in astrocytes: implications for disease spreading and motor neuron pathology in  
812 amyotrophic lateral sclerosis., *J. Biol. Chem.* 288 (2013) 15699–711.  
813 <https://doi.org/10.1074/jbc.M112.425066>.
- 814 [59] G. Wang, M. Dinkins, Q. He, G. Zhu, C. Poirier, A. Campbell, M. Mayer-Proschel, E.  
815 Bieberich, Astrocytes Secrete Exosomes Enriched with Proapoptotic Ceramide and  
816 Prostate Apoptosis Response 4 (PAR-4), *J. Biol. Chem.* 287 (2012) 21384–21395.  
817 <https://doi.org/10.1074/jbc.M112.340513>.
- 818 [60] R.-D. Gosselin, P. Meylan, I. Decosterd, Extracellular microvesicles from astrocytes  
819 contain functional glutamate transporters: regulation by protein kinase C and cell  
820 activation., *Front. Cell. Neurosci.* 7 (2013) 251. <https://doi.org/10.3389/fncel.2013.00251>.
- 821 [61] A.R. Taylor, M.B. Robinson, D.J. Gifondorwa, M. Tytell, C.E. Milligan, Regulation of  
822 heat shock protein 70 release in astrocytes: Role of signaling kinases, *Dev. Neurobiol.* 67  
823 (2007) 1815–1829. <https://doi.org/10.1002/dneu.20559>.
- 824 [62] S. Wang, F. Cesca, G. Loers, M. Schweizer, F. Buck, F. Benfenati, M. Schachner, R.  
825 Kleene, Synapsin I Is an Oligomannose-Carrying Glycoprotein, Acts As an  
826 Oligomannose-Binding Lectin, and Promotes Neurite Outgrowth and Neuronal Survival

- 827           When Released via Glia-Derived Exosomes, *J. Neurosci.* 31 (2011) 7275–7290.  
828           <https://doi.org/10.1523/JNEUROSCI.6476-10.2011>.
- 829 [63] H. Zhao, R. Ding, X. Zhao, Y. Li, L. Qu, H. Pei, L. Yildirimer, Z. Wu, W. Zhang,  
830           Graphene-based nanomaterials for drug and/or gene delivery, bioimaging, and tissue  
831           engineering, *Drug Discov. Today.* 22 (2017) 1302–1317.  
832           <https://doi.org/10.1016/j.drudis.2017.04.002>.

Journal Pre-proof

**HIGHLIGHTS**

Graphene oxide interferes with cell membrane dynamics and enhance astrocytes' release of MVs

MVs driven by graphene oxide stimuli display a different protein profile from chemically driven ones

MVs released upon graphene oxide exposure affect neuronal signaling and membrane stiffness

Journal Pre-proof

# Shedding Plasma Membrane Vesicles Induced by Graphene Oxide Nanoflakes in Brain Cultured Astrocytes

*Mattia Musto<sup>1†</sup>, Pietro Parisse<sup>2</sup>, Maria Pachetti<sup>2</sup>, Christian Memo<sup>1</sup>, Giuseppe Di Mauro<sup>1</sup>,  
Belen Ballesteros<sup>3</sup>, Neus Lozano<sup>3</sup>, Kostas Kostarelos<sup>3,4</sup>, Loredana Casalis<sup>2\*</sup> and Laura  
Ballerini<sup>1\*</sup>*

<sup>1</sup>International School for Advanced Studies (SISSA), 34136 Trieste, Italy

<sup>2</sup>ELETTRA Synchrotron Light Source, 34149 Basovizza, Italy

<sup>3</sup>Catalan Institute of Nanoscience and Nanotechnology (ICN2), Campus UAB, Bellaterra,  
08193 Barcelona, Spain

<sup>4</sup>Nanomedicine Lab, National Graphene Institute and Faculty of Biology, Medicine & Health  
The University of Manchester, Manchester M13 9PT, United Kingdom

## **Conflict of interest**

Authors declare no competing interests.